Nonlinear Instability Mechanism in 3D Collisional Drift-Wave Turbulence

D. Biskamp and A. Zeiler,
Max Planck Institut für Plasmaphysik, EURATOM Association, 85748 Garching, Germany
(Received 19 August 1994)

Numerical simulations of 3D collisional drift-wave turbulence reveal a behavior basically different from that found in previous 2D studies. The linear instability saturates due to energy transfer to small k_z leading to the formation of convective cells. The turbulence is sustained by nonlinear transfer processes between $k_z = 0$ and $k_z \neq 0$ modes, the latter acting as a catalyst. The system tends to relax to a nonturbulent poloidal shear flow.

PACS numbers: 52.35.Ra, 52.35.Kt, 52.35.Mw

Two-dimensional approximations are often used in turbulence studies primarily because they can be treated numerically with much higher resolution than the fully 3D equations, though the physical properties of the 2D system may be basically different from the 3D behavior, the best known example being Navier-Stokes turbulence. On the other hand, incompressible magnetohydrodynamic turbulence shows a rather close relationship between 2D and 3D [1], in particular, in the presence of a strong magnetic field, which introduces anisotropy making the turbulent dynamics quasi-two-dimensional. A similar situation arises in drift-wave turbulence in an inhomogeneous magnetized plasma, i.e., small-scale (compared with the average density gradient scale length) density and electric potential fluctuations, which are believed to play an important role in the transport behavior of magnetically confined plasmas. Because of the basic anisotropy with respect to the magnetic field, two-dimensional modeling of drift-wave turbulence appears to be a good approximation. We will, however, show that this is generally not the case, using the simple system of collisional drift waves in an unsheared magnetic field introduced by Hasegawa and Wakatani [2]. Neglecting ion temperature effects, this model consists of two equations for the electric potential φ and the density fluctuation n, the ion equation of motion

$$\frac{n_0}{\Omega_i}\frac{c}{B_0}(\partial_t\omega + \mathbf{v}\cdot\nabla\omega) = \frac{1}{e}\nabla_\parallel j_\parallel + D^\omega \qquad (1)$$

and the electron continuity equation

$$\partial_t n - n_0'\frac{c}{B_0}\partial_y\varphi + \mathbf{v}\cdot\nabla n = \frac{1}{e}\nabla_\parallel j_\parallel + D^n, \qquad (2)$$

where $\mathbf{v} = (c/B_0)\hat{\mathbf{z}}\times\nabla\varphi, \omega = \nabla_\perp^2\varphi$, n_0 is the background electron density, and $n_0' = -n_0/L_n < 0$ the mean density gradient assumed along the negative x direction. The parallel electric current density $j_\parallel$ is obtained from Ohm's law

$$j_\parallel = \frac{1}{\eta}\left(\frac{1}{en}\nabla_\parallel p_e - \nabla_\parallel\varphi\right), \qquad (3)$$

where $\eta = \nu_{ei}/\omega_{pe}^2$ is the resistivity. Introducing the standard drift-wave normalizations $\varphi \to (e\varphi/T_e)L_n/\rho_s$, $n \to (n/n_0)L_n/\rho_s$, $t \to tc_s/L_n$, $\nabla_\perp \to \rho_s\nabla_\perp$, $\nabla_\parallel \to L_\parallel\nabla_\parallel$, with $L_\parallel$ a typical parallel wavelength or correlation length, Eqs. (1) and (2) become

$$\partial_t\omega + \mathbf{v}\cdot\nabla\omega = \nabla_\parallel^2(n-\varphi) + D^\omega, \qquad (4)$$

$$\partial_t n + \partial_y\varphi + \mathbf{v}\cdot\nabla n = \nabla_\parallel^2(n-\varphi) + D^n, \qquad (5)$$

Here the coefficients in the parallel diffusion terms on the right-hand sides have been chosen as unity, which defines the parallel scale length $L_\parallel$,

$$L_\parallel = (L_n T_e/m_e c_s\nu_{ei})^{1/2}.$$

D^ω and D^n represent perpendicular viscous dissipation effects, which in the present context should only guarantee regularity of φ, n. Since we want to localize these effects at the smallest scales, D^ω, D^n are—rather arbitrarily—chosen as $D^\omega = \mu\nabla_\perp^{(6)}\omega$, $D^n = \nu\nabla_\perp^{(6)}n$, with $\mu = \nu$.

The nonlinear terms $\mathbf{v}\cdot\nabla\omega$ and $\mathbf{v}\cdot\nabla n$ conserve the kinetic energy $E^K = \int v^2\,dV$ and the energy of the density fluctuations $E^N = \int n^2\,dV$, respectively. Switching on the remaining terms the following quadratic forms of n and φ behave in a particularly simple way, the total energy $E = \frac{1}{2}\int(v^2 + n^2)\,dV$ and the generalized enstrophy $W = \frac{1}{2}\int(n-\omega)^2\,dV$, which follow the equations

$$\frac{dE}{dt} = \Gamma - \int[\nabla_\parallel(n-\varphi)]^2\,dV - \mu\int[(\nabla_\perp^2\omega)^2 + (\nabla_\perp\nabla_\perp^2 n)^2]\,dV, \qquad (6)$$

$$\frac{dW}{dt} = \Gamma - \mu\int[\nabla_\perp\nabla_\perp^2(n-\omega)]^2\,dV, \qquad (7)$$

where $\Gamma = \int n v_x\,dV = -\int n\partial_y\varphi\,dV$ is the volume-integrated turbulent plasma flux. Only the Γ term may be positive and hence drive the turbulence by extracting energy from the (fixed) mean density gradient.

Studies of the Hasegawa-Wakatani (HW) equations (4) and (5) have previously been restricted mainly to two-dimensional geometry [3–5] by assuming $\nabla_\parallel^2 \to -k_\parallel^2 = -k_z^2$ to be a constant, proportional to the so-called adiabaticity parameter C (large values of C enforce a nearly adiabatic behavior of the density, $n \simeq \phi$, whence the name). For sufficiently weak viscous dissipation the last term in Eq. (6) is found to be negligible, such that Γ and

 0031-9007/95/74(5)/706(4)$06.00

resistive dissipation balance each other in stationary turbulence, while the viscous term in Eq. (7) remains finite. The spectral properties of stationary 2D HW turbulence have recently been studied for a broad range of C values [4,5]. In all cases one finds a maximum of the angle-integrated energy spectrum $E_k = \int E_{\mathbf{k}}\, d\Omega_{\mathbf{k}}$ at $k = k_0$, where $k_0 \simeq 1$ for $C \sim 1$, and k_0 decreases for both decreasing C, where $k_0 \simeq k_m$, the mode of maximum linear growth rate, and for increasing C, where $k_0 < k_m$. Hence in 2D the HW system does not exhibit an inverse cascade and condensation at small k, contrary to the behavior of the Hasegawa-Mima equation [6], to which the HW equations reduce in the limit $C \to \infty$, i.e., $n \to \varphi$. This can be understood in the sense that for the stationary spectrum $k_m \to 0$ in this limit. Since for larger C the system needs longer and longer times to set up a stationary spectrum down to k_m, this corresponds to an inverse cascade in the limit $C \to \infty$. Because of the rather arbitrary choice of $k_z = \text{const}$ and the strong dependence of the system on the parameter C, it is interesting to consider the 3D HW system, where there is no free parameter, the k_z spectrum being determined self-consistently. It is shown in the present work that the 3D behavior is basically different from that of a 2D finite-C system, the nonlinear energy transfer in k_z playing a dominant role.

Several studies of 3D drift-wave turbulence have previously been performed. In Ref. [7] collisionless drift-wave turbulence was investigated by particle simulation. It has been found that $k_z \neq 0$ drift waves lead to excitation of $k_z = 0$ convective cells. However, since the mean density profile is not kept constant, quasilinear effects prevent the setup of a quasistationary turbulence level, and the spatial resolution used is relatively low. In Ref. [8] the HW equations were solved in a cylindrical plasma including magnetic shear and curvature. The main result was the generation of a poloidal shear flow. As we will see, this behavior is already described by the simple slab model ignoring magnetic shear and curvature, where $k_z = k_\parallel = 0$ modes (interchange modes or convective cells) are linearly stable, but are excited by the nonlinear transfer processes.

The 3D HW equations (4) and (5) are solved in a rectangular box of size $2\pi L_x \times 2\pi L_y \times 2\pi L_z$ with periodic boundary conditions using a pseudospectral method according to the 2/3 rule. The number of modes (or collocation points) are $N_x = N_y = 96$, $N_z = 48$, and the hyperviscosity $\mu = 10^{-4}$, which is small enough to concentrate dissipation at high k in the energy and enstrophy spectra, but still prevents spectral accumulation at high k. Modes are linearly unstable for $k_z \neq 0$ and sufficiently small $k_\perp$ and stable at large $k_\perp$ due to viscous damping. For the parameters given above the maximum growth rate $\gamma_{\max} = 0.15$ is found at $k_x = 0$, $k_y \simeq 1$, and $k_z \simeq 0.5$. (For details of the linear stability properties see, e.g., Ref. [3].) In these 3D computations spatial resolution is necessarily smaller than in previous 2D runs [4,5], where up to 1024^2 modes have been used. Therefore the focus is not on small-scale spectral properties but on the dynamics of the dominant large-scale eddies. In our standard case the dimensions of the computed system are $L_x = L_y = 6$, which is large enough to allow formation of structures $\gg \rho_s$ ($k_{\perp\min}\rho_s = 0.16$). The parallel dimensions $L_z = 6$ are chosen such as to locate the most unstable mode in the lower half ($n_z = 3$) of the k_z spectrum. The time step Δt is determined by the requirement that the energy balance (6) be satisfied with sufficient accuracy. A typical run is illustrated in Fig. 1. The initial state is given by a low level random noise of $\varphi_{\mathbf{k}}$ and $n_{\mathbf{k}}$. Owing to the linear instability the fluctuation energy grows exponentially up to time $t \simeq 70$, when nonlinear effects lead to a bendover. We can identify the nonlinear (quasi)saturation mechanism by considering the energy spectrum $E(k_z) = \sum_{\mathbf{k}_\perp} E_{\mathbf{k}}$, shown in Fig. 2. During the linear instability the spectrum $E(k_z)$ has a maximum at $k_z \sim 0.5$, but for $t > 70$ the maximum of $E(k_z)$ is shifted to smaller k_z. Hence the bendover is due to a nonlinear transfer in k_z from the linearly most strongly driven modes to weakly or nondriven ones leading to the formation of convective cells. The properties in the nonlinear phase are illustrated by the transfer rates of kinetic and density fluctuation energies,

$$T^K(k_z) = \mathrm{Re}\left\{\sum_{k_\perp k'} \hat{\mathbf{z}} \cdot (\mathbf{k} \times \mathbf{k}')k'^2 \varphi_{\mathbf{k}'}\varphi_{\mathbf{k}-\mathbf{k}'}\varphi_{-\mathbf{k}}\right\}, \quad (8)$$

$$T^N(k_z) = \mathrm{Re}\left\{\sum_{k_\perp, k'} \hat{\mathbf{z}} \cdot (\mathbf{k} \times \mathbf{k}')n_{\mathbf{k}'}\varphi_{\mathbf{k}-\mathbf{k}'}n_{-\mathbf{k}}\right\}, \quad (9)$$

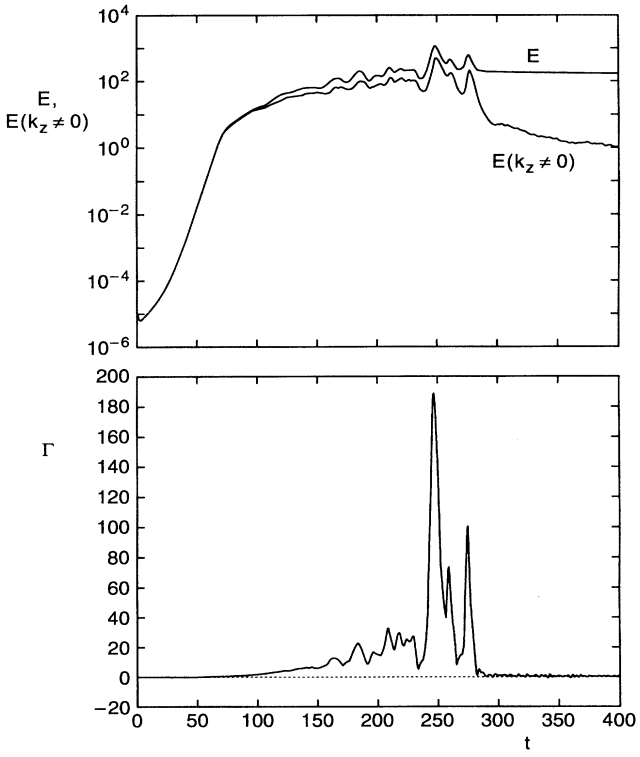

FIG. 1. Time evolution of (a) the total turbulence energy E, the drift-wave energy $E(k_z \neq 0)$, and the turbulent flux Γ.

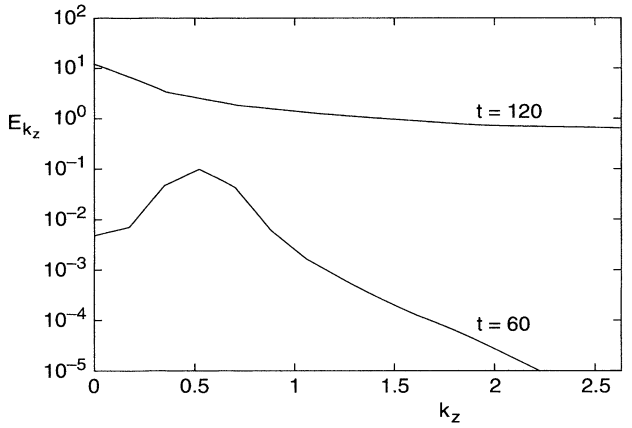

FIG. 2. Energy spectrum $E(k_z)$ in the linear instability phase $t = 60$ and in the nonlinear phase $t = 100$.

plotted in Fig. 3 for $t = 240$, a typical time in this nonlinear phase. Since $T^N(0) < 0$, there is a strong transfer of E_k^N from $k_z = 0$ to $k_z \neq 0$, where $T^N(k_z)$ is almost uniformly distributed and thus drives a broad spectrum of rather high-k_z modes. On the other hand, one finds an inverse transfer of kinetic energy E_k^K from high to small k_z, in particular to $k_z = 0$. Hence in contrast to the linear instability the turbulence energy is primarily generated by the convection of the density at $k_z = 0$. Since there is no linear coupling to the potential

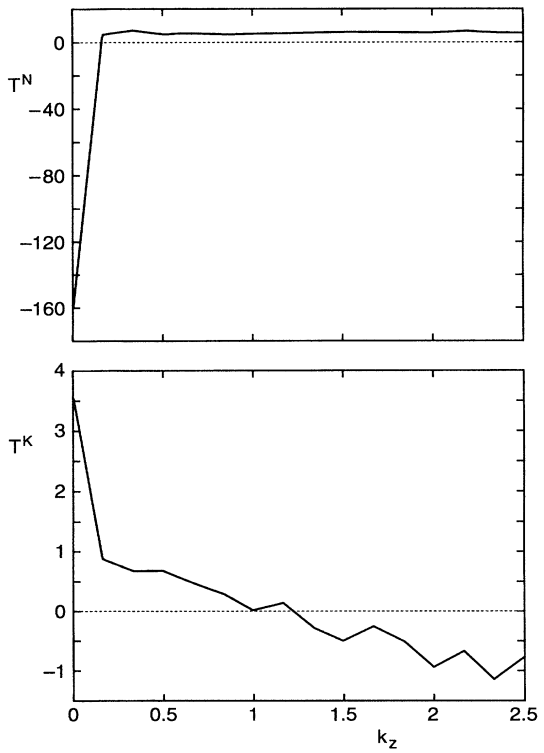

FIG. 3. Density and kinetic energy transfer functions $T^N(k_z), T^K(k_z)$ in the phase of strong turbulence $t = 240$.

at $k_z = 0$, a nonlinear process involving $k_z \neq 0$ modes is needed, the latter acting as a kind of catalyst. In this nonlinear process both convective cells $E(k_z = 0)$ and drift waves $\sum_{k_z \neq 0} E(k_z)$ are growing. The nonlinear process is illustrated in Fig. 4. Large-scale convective cells drive $k_z = 0$ density fluctuations at broad scales $k_\perp$. These excite $k_z \neq 0$ drift waves, which in turn reinforce the convective cells. For $k_z \neq 0$ the $k_\perp$ spectrum still follows roughly the behavior of the linear growth rate with a maximum at finite $k_\perp$. It is interesting to note that only for $k_z \gg 1$, $k_\perp \ll 1$ the fluctuations are nearly adiabatic $n_k \simeq \varphi_k$. While for $k_z \ll 1$, $k_\perp \ll 1$ one finds $\varphi_{\mathbf{k}} \gg n_{\mathbf{k}}$, density fluctuations dominate $n_{\mathbf{k}} \gg \varphi_{\mathbf{k}}$ for $k_z, k_\perp \gtrsim 1$.

In the state dominated by large-scale convective cells, which give rise to strong energy fluctuations ($t \simeq 240$–280), there is the tendency of condensation to the $k_y = 0$ mode corresponding to a poloidal shear flow. The mechanism is related to that described in Ref. [9]. A main feature of this process, which occurs at $t \simeq 280$, is the quenching of the nonlinear instability described above, since the driving force $\Gamma \propto k_y$ in Eqs. (6) and (7) (corresponding to the vertical arrow in Fig. 4) is switched off. The small-scale drift-wave turbulence decays, since dissipation now exceeds the reduced nonlinear transfer rate. As the result the system relaxes to a quasilaminar stationary poloidal flow. (It should be noted that because of the nonuniform velocity shear—the essentially sinusoidal flow profile has two points of vanishing shear—the turbulence does not decay to arbitrarily low amplitudes. Assuming a fixed sinusoidal shear flow results in a stationary rather low nonlinear level of drift waves located around these points.)

In the present model system imbedded in a homogeneous magnetic field the poloidal shear flow is Kelvin-Helmholtz unstable, if the aspect ratio fo the computational box L_y/L_x exceeds unity. Hence for $L_y/L_x > 1$ the poloidal shear flow cannot be set up. Instead the system settles into a turbulent shear flow state in the x direction ($k_x = 0$), which is possible because of the pe-

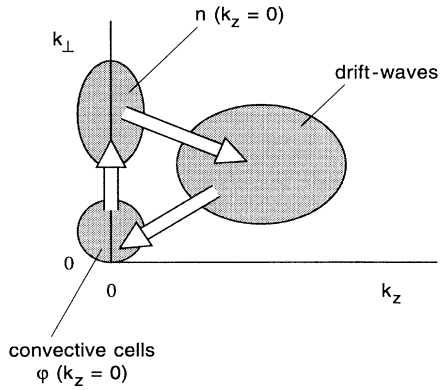

FIG. 4. Schematic illustration of the nonlinear instability mechanism.

riodic boundary conditions used. In this case Γ is not switched off, the nonlinear instability remains active giving rise to continued growth of both convective cells and drift waves. Since in a tokamak plasma the poloidal shear flow is Kelvin-Helmholtz stabilized by the poloidal magnetic field [10], we concentrate on the case $L_y/L_x \leq 1$, where the poloidal flow is stable.

In a real toroidal plasma column a poloidal flow is damped collisionally due to magnetic pumping [11]. Modeling the effect we introduce at $t = 400$ a damping term $-\alpha\omega_{\mathbf{k}}$ into Eq. (1) for modes with either $k_y = 0$ or $k_x = 0$. We find that during the period $t \simeq 400$–440 the shear flow decays to a low amplitude, which reintroduces the turbulent flux Γ and in its wake the drift-wave turbulence. The dynamic state is similar to that in the first turbulent phase $t = 200$–280 and terminates by the regeneration of a poloidal shear flow state, which again suppresses the nonlinear instability and the turbulent flux. This behavior of alternating periods of shear flow and turbulence, appearing in a burstlike manner, continues; see Fig. 5.

In conclusion, we have shown that 3D collisional drift-wave turbulence is basically different from the behavior of a 2D system with a given adiabaticity parameter C. The turbulence is not driven by the linear instability mechanism, but by a nonlinear process. Large-scale convective cells excite $k_z = 0$ density fluctuations. From these fluctuations energy is transferred to a broad spectrum of $k_z \neq 0$ drift waves, where the energy is partly dissipated and partly transferred back to the convective cells. There is an inherent tendency to generate a shear flow, either in poloidal direction ($k_y = 0$), or, if this flow is Kelvin-Helmholtz unstable, in radial direction ($k_x = 0$). In the case of a poloidal shear flow the turbulent flux Γ is switched off leading to rapid turbulence decay. Introducing an explicit damping of the shear flow, representing the effect of magnetic pumping in a toroidal plasma column, generates an intermittent turbulent state, where laminar periods of almost zero flux alternate with turbulent periods of large flux. The transitions occur very rapidly on time scales shorter than the linear growth times. This behavior may be related to the grassy ELM's [12] observed in tokamak plasmas.

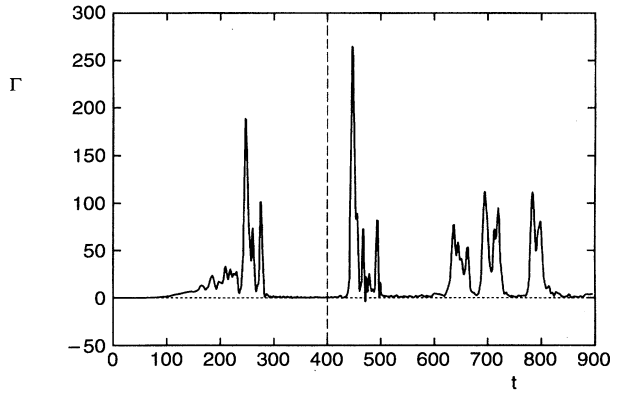

FIG. 5. Time evolution of Γ for the same run as shown in Fig. 1, continued at $t = 400$ with a shear flow damping $\alpha = 10^{-2}$.

The authors are grateful to Dr. J. Drake for several useful discussions.

[1] See, e.g., D. Biskamp and H. Welter, Phys. Fluids B **1**, 1964 (1989).
[2] A. Hasegawa and M. Wakatani, Phys. Rev. Lett. **50**, 682 (1983); M. Wakatani and A. Hasegawa, Phys. Fluids **27**, 611 (1984).
[3] A. E. Koniges, J. A. Crotinger, and P. H. Diamond, Phys. Fluids B **4**, 2785 (1992).
[4] D. Biskamp, S. J. Camargo, and B. D. Scott, Phys. Lett. A **186**, 239 (1994).
[5] S. J. Camargo, D. Biskamp, and B. D. Scott, Phys. Plasmas (to be published).
[6] A. Hasegawa, C. G. Maclennen, and Y. Kodama, Phys. Fluids **22**, 2122 (1979).
[7] C. Z. Cheng and H. Okuda, Phys. Rev. Lett. **38**, 708 (1977), Nucl. Fusion **18**, 587 (1978).
[8] A. Hasegawa and M. Wakatani, Phys. Rev. Lett. **59**, 1581 (1987).
[9] J. M. Finn, J. F. Drake, and P. N. Guzdar, Phys. Fluids B **4**, 2758 (1992).
[10] See, e.g., S. Chandrasekhar, *Hydrodynamic and Hydromagnetic Stability* (Dover, New York, 1981); B. D. Scott, P. W. Terry, and P. H. Diamond, Phys. Fluids **31**, 1481 (1988).
[11] See, e.g., A. B. Hassam and R. M. Kulsrud, Phys. Fluids **21**, 2271 (1978).
[12] See, e.g., T. Ozeki *et al.*, Nucl. Fusion **30**, 1425 (1990).